63rd International Astronautical Congress, Naples, Italy.

IAC-12-C1.4.2

HYBRID LOW-THRUST TRANSFERS TO EIGHT-SHAPED ORBITS FOR POLAR OBSERVATION

Jeannette Heiligers
Advanced Space Concepts Laboratory, University of Strathclyde, Glasgow, United Kingdom,
jeannette.heiligers@strath.ac.uk

Matteo Ceriotti
Systems Power and Energy division, School of Engineering, University of Glasgow, United Kingdom,
matteo.ceriotti@glasgow.ac.uk

Colin R. McInnes
Advanced Space Concepts Laboratory, University of Strathclyde, Glasgow, United Kingdom,
colin.mcinnes@strath.ac.uk

In this paper, transfers from low Earth orbit (LEO) to so-called eight-shaped orbits at the collinear libration points in the circular restricted three-body problem are investigated. The potential of these orbits (both natural and sail displaced) for high-latitude observation and telecommunication has recently been established. The transfer is modelled by distinguishing between a near-Earth phase and an interplanetary phase. The near-Earth phase is first assumed to be executed with the Soyuz Fregat upper-stage, which brings the spacecraft from LEO to a highly elliptic orbit. From there, the interplanetary phase is initiated which uses low-thrust propulsion to inject the spacecraft into one of the eight-shaped orbit's manifolds. Both solar electric propulsion (SEP), solar sailing and hybridised SEP and solar sailing are considered for this phase. The objective is to maximise the mass delivered to the eight-shaped orbit starting from a realistic Soyuz launch vehicle performance into LEO. Optimal trajectories are obtained by solving the optimal control problem in the interplanetary phase with a direct pseudospectral method. The results show that (over the full range of propulsion techniques) 1564 to 1603 kg can be injected into a natural eight-shaped orbit. Within this relatively small range, hybrid propulsion performs best in terms of mass delivered to the eight-shaped orbit, while SEP enables the fastest transfer times. With the interplanetary phase optimised, the upper-stage near-Earth phase is replaced by a multi-revolution low-thrust spiral. Locally optimal control laws for the SEP thruster and solar sail are derived to minimise the time of flight in the spiral. Both pure SEP and hybrid spiral show a significant reduction in the mass required in LEO to deliver the spacecraft to the eight-shaped orbits. While hybrid propulsion did not stand out for the use of an upper-stage near-Earth phase, it does for the use of a low-thrust spiral as it significantly reduces the spiral time with respect to the pure SEP case.

I. INTRODUCTION

Research in the field of novel concepts for space based polar observation is flourishing. The driving factor behind theses developments is the need to improve the data that can be obtained from current infrastructure such as highly inclined low Earth orbits and Molniya orbits. The first provide poor temporal resolution data as the spacecraft can only view a narrow swath of the polar regions during each orbital passage, while the second, despite having a better temporal resolution, have a too low inclination for high-latitude coverage. Improving the observation conditions is crucial for applications such as the identification of changes in the polar environment in terms of sea-ice coverage and thickness to support analyses of long-term climate trends. Other applications of polar data include high-latitude telecommunications, weather forecasting and ship navigations.[1] These are of importance for ongoing research activities in the Antarctic and increased shipping activity which can be expected from Arctic oil and gas exploitation[2] and the fact that the northern sea routes are opening up.[3]

In response to the need for improved polar observation, the literature shows a wealth of novel concepts, including polar Molniya orbits,[4] pole-sitter

orbits,[5] and concepts that rely on artificial equilibria such as non-Keplerian orbits displaced above the ecliptic.[6, 7] Recently, to complement these concepts, a new concept for polar observation has been introduced that makes use of eight-shaped vertical Lyapunov orbits.[8] These orbits exist in the vicinity of the collinear Lagrange points in the circular restricted three-body problem (CR3BP).[9, 10] The name eight-shaped orbits comes from the fact that, viewed in the *yz*-plane of the CR3BP, the orbit resembles a figure of eight. Since the spacecraft spends most of its time at the apices of this figure of eight, which bend over the polar regions for a range of out-of-plane amplitudes, eight-shaped orbits can enhance future high-latitude Earth observation and telecommunication missions.

The design of these eight-shaped orbits, both natural and solar sail displaced ones, as well as a polar visibility analysis and stability analysis was performed by Ceriotti and McInnes.[8] This paper will complement that study by investigating optimal low-thrust transfers from low Earth orbit (LEO) to these eight-shaped orbits. For that, the work in this paper will build upon, and extend, previous work on low-thrust transfers to eight-shaped orbits by Senent and co-authors:[11] like the work by Senent, this paper will exploit a combination of low-thrust propulsion and the manifold structure of the eight-shaped orbits. However, while Reference 11 considers minimum time transfers (for a fixed mass ratio), this paper investigates transfers that maximise the mass delivered to the eight-shaped orbits. Furthermore, rather than solving the optimal control problem with an indirect method, a direct method is employed. Also, by considering the launch capability of the Soyuz launch vehicle, realistic performances in terms of mass delivered to the eight-shaped orbit are obtained. Finally, a range of propulsion techniques will be considered, including solar electric propulsion (SEP) (as Reference 11), but also solar sailing and hybridised SEP and solar sailing. The latter has shown promising results for a range of applications[12-15] as it overcomes the limitations of the individual propulsion systems (e.g. the SEP thruster complements the solar sail by enabling a thrust in the direction of the Sun which the sail is unable to generate).

The approach to the design of optimal low-thrust transfers to the eight-shaped orbits makes use of a decoupling of a transfer phase close to the Earth, which (for the use of low-thrust propulsion) results in a multi-revolution spiral, and the interplanetary phase. The first, near-Earth, phase will initially be designed as a two-body Soyuz Fregat upper-stage transfer from a fixed inclination, low Earth parking orbit up to insertion into the interplanetary phase. From there, the motion of the spacecraft is considered in the CR3BP and low-thrust propulsion is used to deliver the spacecraft to one of the manifolds of the eight-shaped orbit, which will subsequently ballistically deliver the spacecraft to the eight-shaped orbit. As noted, the objective is to maximise the mass delivered to the eight-shaped orbit, by making full use of the launch vehicle performance into LEO. The controls in this optimal control problem are the thrust profile in the interplanetary transfer phase as well as the particular manifold and the position along the manifold at which the spacecraft is inserted. This optimal control problem is solved using a direct pseudospectral method which links the near-Earth and interplanetary phases in an event constraint. To assess the performance of the different propulsion techniques and to provide an initial guess to solve the optimal control problem, ballistic transfers that exploit particular manifolds that closely pass by the Earth will also be considered. The second step in the approach is to replace the high-thrust upper-stage transfer from LEO to the interplanetary phase by a minimum time spiral trajectory. To model the multi-revolution, long duration spiral, locally optimal control laws for the SEP thruster and the solar sail are employed to efficiently increase the semi-major axis, eccentricity and inclination. The optimal control problem in the spiral is subsequently solved using the same direct pseudo-spectral method as used for optimising the interplanetary phase.

The structure of this paper is as follows: first the system dynamics in the CR3BP, which will be used for the definition of the eight-shaped orbits as well as for the interplanetary transfer phase, will be provided. Subsequently, a definition of the eight-shaped orbits, the selection of two particular orbits that will be considered in this paper and the generation of manifolds winding onto these orbits will be presented. Then, the design approach will be outlined for the case of a Fregat upper-stage near-Earth phase, the optimal control problem will be derived and the results for ballistic, SEP, solar sail and hybrid propulsion will be presented. Finally, the design approach for the case of a low-thrust near-Earth spiral phase will be discussed and the results will be presented. The paper finishes with conclusions.

II. SYSTEM DYNAMICS

Both the eight-shaped orbit itself as well as the interplanetary transfer phase are defined in the circular restricted three body problem, which describes the motion of an infinitely small mass, m, (i.e. the spacecraft) under the influence of the gravitational attraction of two much larger, primary masses, m_1 and m_2. The gravitational influence of the small mass on the larger masses is neglected and the larger masses are assumed to move in circular orbits about their common centre of mass. In this paper, the primary masses are the Sun and Earth. Furthermore, the motion is described in a reference frame that has the origin in the centre of mass, the x-axis connects the larger masses and points in the direction of the smaller of the two, m_2, while the z-axis is directed perpendicular to the plane in which the two larger masses move. The y-axis completes the right-handed reference frame. Finally, the frame rotates at constant angular velocity, ω, about the z-axis. See also Fig. 1.

New units are introduced: the sum of the two primaries is taken as unit of mass, i.e. $m_1+m_2 = 1$. Then, with the mass ration $\mu = m_2/(m_1+m_2)$, which equals 3.0404×10^{-6} for the Sun/Earth system, the masses of the larger bodies become $m_1 = 1-\mu$ and $m_2 = \mu$. As unit of length, the distance between the main bodies is selected, and $1/\omega$ is chosen as unit of time, yielding $\omega = 1$ and so one year is represented by 2π. In this reference frame, the motion of the mass m, i.e. the spacecraft, is described by:[16]

$$\ddot{\mathbf{r}} + 2\boldsymbol{\omega}\times\dot{\mathbf{r}} + \nabla U = \mathbf{a} \tag{1}$$

and

$$U = -\frac{x^2+y^2}{2} - \left(\frac{1-\mu}{r_1} + \frac{\mu}{r_2}\right) \tag{2}$$

with $\mathbf{r}$, r_1 and r_2 the position vectors with respect to the barycentre, the first primary and the second primary, and $\mathbf{a}$ is a thrust-induced acceleration. For a ballistic transfer or orbit, $\mathbf{a}$ is zero, while for an SEP, a solar sail[17] or a hybrid system, the acceleration is given by:

$$\mathbf{a}_{SEP} = \frac{\mathbf{T}}{m} \tag{3}$$

$$\mathbf{a}_s = \beta_0 \frac{1-\mu}{r_1^2}\left(\hat{\mathbf{n}}\cdot\hat{\mathbf{r}}_1\right)^2 \hat{\mathbf{n}} \tag{4}$$

$$\mathbf{a}_h = \frac{\mathbf{T}}{m} + \beta_0 \frac{m_0}{m}\frac{1-\mu}{r_1^2}\left(\hat{\mathbf{n}}\cdot\hat{\mathbf{r}}_1\right)^2 \hat{\mathbf{n}} \tag{5}$$

In these equations, $\mathbf{T}$ is the SEP thrust vector and $\mathbf{n}$ is the normal vector of the solar sail. Both are defined in the reference frame defined in Fig. 1. Furthermore, β_0 is the solar sail lightness number (which is proportional to the area-to-mass ratio of the sailcraft).[17] For near-term systems an SEP thrust magnitude of 0.2 N can be assumed (e.g. the EADS/Astrium RIT-XT thruster)[18] and for the solar sail, lightness numbers of up to 0.05 can be considered feasible in the near-term.[19] Note that the solar sail is unable to generate a thrust component in the direction of the Sun. The angle between the normal vector of the sail and the Sun-sail vector can therefore not exceed 90°, or equivalently, $\left(\hat{\mathbf{n}}\cdot\hat{\mathbf{r}}_1\right) > 0$.

Due to the consumption of propellant in the hybrid propulsion case, the fraction m_0/m is included in the solar sail acceleration in Eq. (5). Furthermore, for the hybrid case, as well as for the pure SEP case, the dynamics in Eq. (1) need to be augmented with the following differential equation for the mass:

$$\dot{m} = -\frac{|\mathbf{T}|}{I_{sp}\, g_0} \tag{6}$$

with g_0 the Earth standard gravitational acceleration and I_{sp} the specific impulse of the SEP thruster, for which a value of 3200 s is assumed.[18]

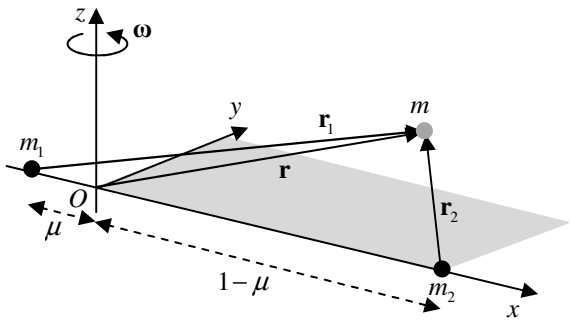

Fig. 1 Circular restricted three body problem reference frame.

III. EIGHT-SHAPED ORBITS

III.I Definition

Defined in the CR3BP, eight-shaped orbits are periodic orbits symmetric both with respect to the xy-plane and the xz-plane. The orbit crosses the xz-plane four times per period, and the x-axis twice, see Fig. 2. More specifically, the state vector at either the most northern or southern point of the orbit, indicated by the index '0', is given through:

$$\mathbf{x}_0 = \begin{bmatrix} x_0 & 0 & z_0 & 0 & \dot{y}_0 & 0 \end{bmatrix}^T \quad (7)$$

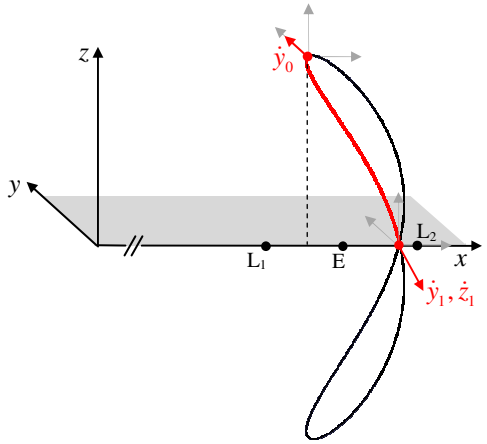

Fig. 2 Schematic of eight-shaped orbit in CR3BP reference frame.

One quarter of the orbit later, at the next intersection with the *xz*-plane, the state vector is:

$$\mathbf{x}_1 = \begin{bmatrix} x_1 & 0 & 0 & 0 & \dot{y}_1 & \dot{z}_1 \end{bmatrix}^T \quad (8)$$

If the conditions in Eqs. (7) and (8) are satisfied, an integration of the equations of motion for one full period, guarantees that the orbit is closed and periodic.

Once an eight-shaped orbit is found, families of eight-shaped orbits can be obtained by continuation using a predictor-corrector scheme. Then, the initial state vector defined in Eq. (7) is perturbed in a specified direction and the equations of motion are integrated forward until the first intersection with the *xz*-plane. The conditions at this intersection should satisfy Eq. (8), but most likely will not. A correction to the perturbation of the initial state vector is then applied and a further iterative approach will eventually ensure that Eq. (8) is satisfied. Further details on the generation of eight-shaped orbits can be found in Reference 8.

A selection of the orbits in the family of natural orbits around the L_2-point of the Sun/Earth system is provided in Fig. 3. The figure also includes a cone which represents the motion of the polar axis during the year in the rotating CR3BP reference frame. The figure clearly demonstrates that for particular values of the *z*-amplitude, the apices of the eight-shaped orbits bend over the polar regions and lie within the polar cone. Furthermore, considering the fact that the velocity is lowest at these parts of the orbits, the applications of these orbits for polar observation is clear.

Although Fig. 3 only provides the family of natural eight-shaped orbits in the vicinity of the L_2-point of the Sun/Earth system, a similar set of orbits can be found in the vicinity of the L_1-point. However, the family close to the L_2-point can take advantage of using a solar sail to displace the orbits towards the Sun (and therefore towards the Earth), similarly to the way that the collinear Lagrange points can be displaced towards the Sun.[20] In particular cases this can lead to improved observation conditions.[8] The new families of orbits that originate by orientating the solar sail perpendicular to the Sun-sail line and varying the sail lightness number are depicted in Fig. 4.

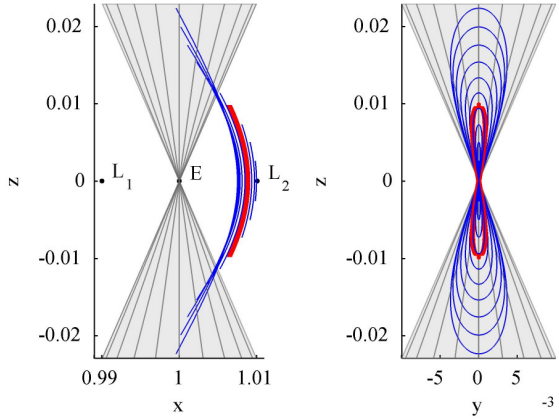

Fig. 3 Family of natural eight-shaped orbits at L_2 with selected natural orbit in red.

III.I Orbit selection

For the analyses in this paper, two particular eight-shaped orbits will be selected. The first belongs to the category of natural eight-shaped orbits and is highlighted in red in Fig. 3. This particular orbit appeared to be advantageous from a trajectory design point of view as will become clear later on in the paper. The second orbit belongs to the class of sail displaced eight-shaped orbits and is highlighted by the solid blue marker in Fig. 4. This orbit, with a sail lightness number of 0.026, appeared to be highly suitable for polar observation: it's period is π (i.e. half a year) such that the same visibility conditions are repeated throughout the year. Furthermore, the apices reach the sunward edge of the polar cone, which means that both Poles can be imaged under highly favourable lighting conditions during the Arctic and Antarctic summers. Using three spacecraft, latitudes above 77°N and 75°S can be observed continuously throughout the year.[8] Details for both selected orbits can be found in Table 1.

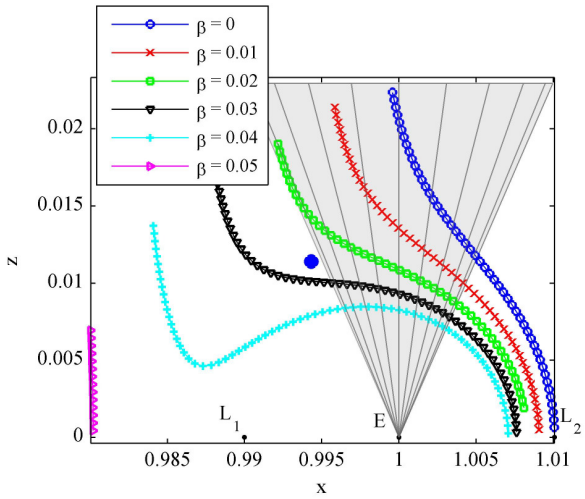

Fig. 4 Families of solar sail displaced eight-shaped orbits at L_2 for different sail lightness numbers, β_0, represented by the most northern point of the orbit. The solid blue marker is the selected sail displaced orbit.

	Natural orbit	Sail displaced orbit
β_0	0	0.026
x_0	1.006470	0.994319
z_0	0.009812	0.011383
$\dot{x}_0$	0.002818	0.010571
Period	1.1059π	π

Table 1 Details of eight-shaped orbits selected in this paper for the design of optimal transfers.

III.III Manifolds

For the design of transfers that maximise the mass delivered to the eight-shaped orbits, the manifolds that wind onto these orbits are of particular interest. The theory of invariant manifolds and the approach to find these manifolds is described extensively in the literature.[21] Summarising, the manifolds, W, of a periodic orbit can be found by perturbing the state vector at any point along the orbit in a particular direction. This direction is given by the eigenvalues and eigenvectors of the Jacobian of the linearised system. The eigenvector associated with the real eigenvalue of magnitude larger than 1, $\mathbf{v}^u$, provides the unstable direction, while the eigenvector associated with the real eigenvalue of magnitude smaller than 1, $\mathbf{v}^s$, provides the stable direction, see Fig. 5. At a state $\mathbf{x}_0$ in the periodic orbit, the initial state vector of the unstable and stable manifolds are then given by:

$$\mathbf{x}_W^u(\mathbf{x}_0) = \mathbf{x}_0 \pm \varepsilon \frac{\mathbf{v}^u(\mathbf{x}_0)}{\left|\mathbf{v}^u(\mathbf{x}_0)\right|} \tag{9}$$

$$\mathbf{x}_W^s(\mathbf{x}_0) = \mathbf{x}_0 \pm \varepsilon \frac{\mathbf{v}^s(\mathbf{x}_0)}{\left|\mathbf{v}^s(\mathbf{x}_0)\right|} \tag{10}$$

where the ±-sign indicates the two directions in which the state vector can be perturbed. Furthermore, ε is the actual perturbation and is set equal to 200 km, which is small enough such that the linear approximation of the system still holds, but large enough so that the time to wind onto or depart from the periodic orbit is not too large due to the asymptotic nature of the manifolds.[21, 22] By forward and backward integration of the initial state vectors in Eqs. (9) and (10), respectively, the unstable and stable manifolds can be generated.

For the orbits in this paper a total of 80 manifolds are generated per eight-shaped orbit.

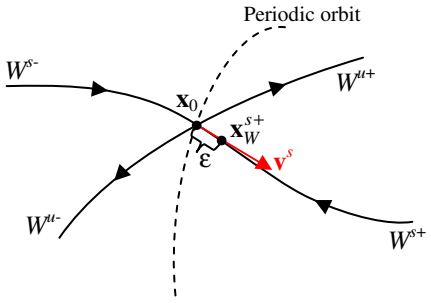

Fig. 5 Schematic of method to generate the two branches of the unstable, W^u, and stable, W^s, manifolds of a periodic orbit.

IV HIGH-THRUST LAUNCH DESIGN APPROACH

A schematic of the design approach when using a Soyuz Fregat upper-stage to depart from LEO is provided in Fig. 7. The figure indicates that the upper-stage delivers the spacecraft to a highly elliptic orbit (hereafter referred to as "target orbit") which marks the end of the near-Earth phase and the start of the interplanetary phase. In the interplanetary phase, low-thrust propulsion is used to deliver the spacecraft to one of the manifolds of the eight-shaped orbits selected in Section III.I, which ensures that the spacecraft will be injected into the eight-shaped orbit. Both phases, the near-Earth and interplanetary phases, will be discussed in more detail in the next two subsections, after which the optimal control problem to be solved in the low-thrust interplanetary phase will be derived.

IV.I Near-Earth phase

While the interplanetary phase and the eight-shaped orbit itself are modelled in the CR3BP (see Section III), the near-Earth phase is modelled using a two-body approximation and in the Earth inertial reference frame shown in Fig. 6: the $x_E y_E$-plane lies in the equatorial plane, the x_E-axis always points to the winter solstice and the z_E-axis is directed along the Earth's polar axis.

Previous work has developed an accurate model to compute the mass that can be delivered by the Fregat upper-stage to a general target orbit starting from LEO.[23] The model was validated by showing that its results match the launch vehicle performance provided by the Soyuz launch manual.[24]

The model starts from the fact that the spacecraft, upper-stage and an adapter are launched into a 200 km altitude circular LEO with one of four reference inclinations, where the launch vehicle performance is largest for the lowest inclination of 51.8°: 7184 kg. The upper-stage is subsequently used to perform a Hohmann-type transfer to the target orbit where any required inclination change is distributed over the first Fregat burn at LEO (15% of required inclination change) and the second Fregat burn at the apogee of the target orbit (85% of required inclination change). Using well-known Hohmann transfer formulas and the rocket equation, the mass delivered to the target orbit can be computed. Additional information required for these computations is provided in Table 2. The only limitation of the model is the fact that the eccentricity of the target orbit (and consequently the state vector at the start of the interplanetary phase, see Fig. 7) cannot exceed unity. This has implications for the optimal control problem as will be discussed in Section IV.III.

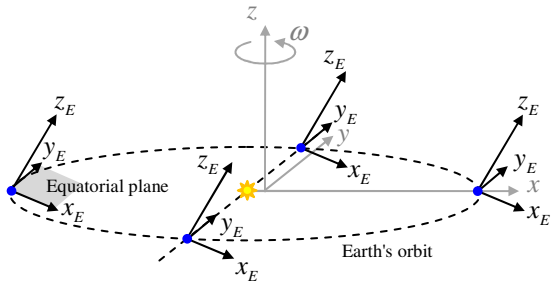

Fig. 6 Schematic of Earth inertial reference frame (in black) used to define the near-Earth phase. The CR3BP frame is depicted in grey for reference.

LEO altitude, km	200
LEO eccentricity	0
LEO inclination, deg	51.8
Soyuz performance into LEO, kg	7185
Fregat mass, kg	1000
Adapter mass, kg	100
Fregat specific impulse, s	330

Table 2 Soyuz parking orbit and launch vehicle specifications.

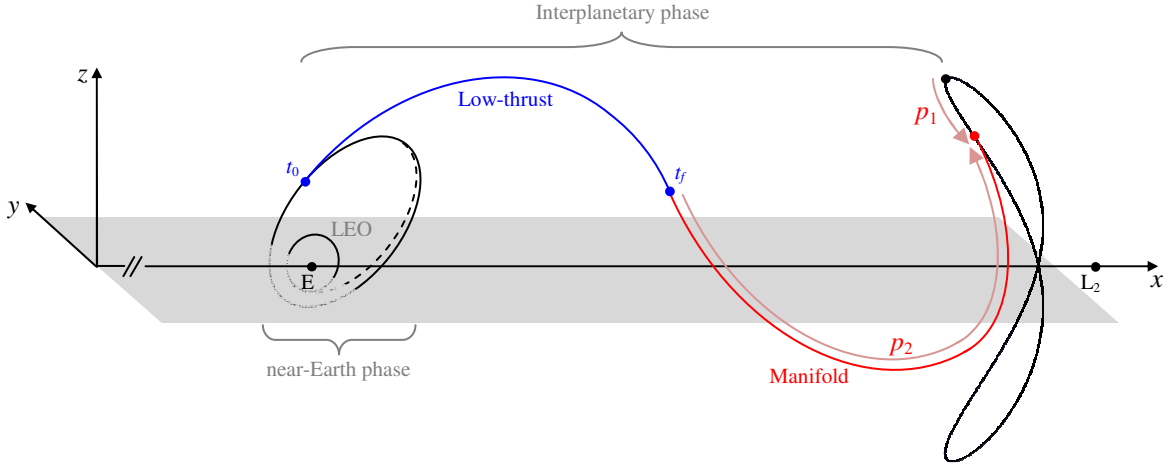

Fig. 7 Schematic of design approach for optimal transfers to eight-shaped orbits employing a high-thrust near-Earth phase.

IV.II Interplanetary phase

The interplanetary phase consists of a low-thrust arc and a manifold arc. The first starts from the target orbit which defines the end of the near-Earth phase, and connects to the manifold arc. The point of connection is defined by two parameters, p_1 and p_2, as indicated in Fig. 7. The first parameter is measured along the eight-shaped orbit and defines the particular manifold that is used for the transfer. The second parameter is used to indicate the length of the manifold arc. It is measured from the point of connection up to injection into the eight-shaped orbit.

IV.III Optimal control problem

As indicated previously, the objective is to maximise the mass injected into the eight-shaped orbit. This is equivalent to optimising the mass delivered to the start of the manifold. To accomplish this objective, the optimal control problem in the low-thrust arc needs to be solved. The time domain in the optimal control problem therefore spans the time between the start and end of this low-thrust arc, which are defined as t_0 and t_f in Fig. 7. The idea is that the initial state vector of the low-thrust arc fully determines the near-Earth phase as the only design variable in the near-Earth phase is the target orbit, which in its turn is defined by the low-thrust arc initial state vector. For this, the initial state vector is transformed from the CR3BP reference frame to the reference frame defined in Fig. 6, and subsequently to Keplerian elements. Clearly, the closer these Keplerian elements are to the Keplerian elements of the LEO, the more mass can be injected into the interplanetary phase. Furthermore, the final state vector of the low-thrust arc is defined by the choice for the parameters p_1 and p_2. The optimal control problem will thus search for a thrust profile in the low-thrust arc and for a combination of p_1 and p_2 such that the initial conditions are as favourable as possible. Simultaneously, for a pure SEP or hybrid transfer, the required thrust profile to achieve this should be feasible and should not be too demanding such that a maximum portion of the mass at the start of the low-thrust arc is delivered to the start of the manifold. This optimal control problem is solved using a direct method based on pseudospectral transcription, implemented in the tool PSOPT.[25]

In mathematical form, the optimal control problem is defined as follows. First, the objective function is given by the mass at the end of the low-thrust arc:

$$J = -f_{penalty} m_f \tag{11}$$

The penalty, $f_{penalty}$, is introduced to penalise the objective function in case the eccentricity at the start of the low-thrust arc (and thus of the target orbit in the near-Earth phase) is larger than 1. As indicated previously, the model used in the near-Earth phase only holds for eccentricities smaller than unity. However, it is possible that in its search for the optimal solution, PSOPT tries a solution with eccentricity larger than 1. In order to evaluate the near-Earth phase even in this case, the eccentricity is artificially set to a value smaller than 1 using a smooth step function. However, to ensure that PSOPT discards this option, the penalty is introduced into the objective function by using an additional smooth step function.

The state vector is given by the Cartesian coordinates in the CR3BP reference frame and (in the case of SEP or hybrid propulsion) the mass of the spacecraft:

$$\mathbf{x} = \begin{cases} \begin{bmatrix} x & y & z & \dot{x} & \dot{y} & \dot{z} \end{bmatrix}^T & \text{Solar sail} \\ \begin{bmatrix} x & y & z & \dot{x} & \dot{y} & \dot{z} & m \end{bmatrix}^T & \text{SEP/Hybrid} \end{cases} \tag{12}$$

The dynamics of the spacecraft in the low-thrust arc are provided by Eqs. (3) to (6).

The control vector also depends on the type of propulsion used:

$$\mathbf{u} = \begin{cases} \begin{bmatrix} T_x & T_y & T_z & p_1 & p_2 \end{bmatrix}^T & \text{SEP} \\ \begin{bmatrix} n_x & n_y & n_z & p_1 & p_2 \end{bmatrix}^T & \text{Sail} \\ \begin{bmatrix} T_x & T_y & T_z & n_x & n_y & n_z & p_1 & p_2 \end{bmatrix}^T & \text{Hybrid} \end{cases} \tag{13}$$

where p_1 and p_2 are static control variables, while the SEP thrust vector and sail normal vector components are dynamics control variables. Bounds on these controls can be set as follows:

$$\begin{aligned} -\mathbf{T}_{\max} \le \mathbf{T} \le \mathbf{T}_{\max} \\ -\mathbf{1} \le \mathbf{n} \le \mathbf{1} \\ 0 \le p_1 \le P_o \\ 0 \le p_2 \le 2\pi \end{aligned} \tag{14}$$

with $T_{\max}$ equal to the previously determined value of 0.2 N (see Section II). The period of the eight-shaped orbit, P_o, can be found in Table 1 and from the bound on p_2, it becomes clear that the 'length' of the manifold cannot exceed a transfer time of 2π (i.e. 1 year).

Due to the choice for the controls as the Cartesian coordinates, the following path constraints need to be taken into account:

$$\begin{aligned} &|\mathbf{T}| \le T_{\max} && \text{SEP/Hybrid} \\ &|\mathbf{n}| \le 1 && \text{Sail/Hybrid} \\ &\left(\hat{\mathbf{n}} \cdot \hat{\mathbf{r}}_1\right) \ge 0 && \text{Sail/Hybrid} \end{aligned} \tag{15}$$

Finally, the following event constraints need to be satisfied that link the start and end of the low-thrust arc to the near-Earth phase and the manifold, respectively. The events on the initial state vector are:

$$\begin{aligned} &e_0 < 1 \\ &a_0 < 500\,000 \text{ km} \\ &m_{LEO} \le 7185 \text{ kg} \end{aligned} \tag{16}$$

where the first two constraints (on the eccentricity and semi-major axis) ensure the validity of the near-Earth phase model, while the last event ensures that the mass in LEO does not exceed the maximum mass of 7185 kg (see Table 2).

The event constraints on the final state vector are:

$$\begin{aligned} \mathbf{x}_f &= \mathbf{x}_{M,0}\left(p_1, p_2\right) \\ t_f &= t_{M,0}\left(p_1, p_2\right) = p_1 - \left(2\pi - p_2\right) \end{aligned} \tag{17}$$

The state vector and time at the end of the low-thrust arc should thus coincide with the state vector and time at the start of the manifold, which depend on the values assigned to the two static control variables. The actual value of $\mathbf{x}_{M,0}$ is computed through an interpolation of large state matrices that provides the position and velocity vectors for a range of values for p_1 and p_2, i.e. for a discrete number of locations along each of the manifolds.

V. RESULTS – HIGH-THRUST LAUNCH

V.I Ballistic trajectories

In order to provide an initial guess for the optimal control solver, the option of a ballistic transfer is investigated. In that case, no low-thrust arc exists and the near-Earth phase is directly patched to the manifold at the location where it most closely passes to the Earth. The state vector at that location in the manifold is transformed to the reference frame of Fig. 6 and subsequently into Keplerian elements. Then, the mass that can be injected into the corresponding Keplerian orbit is computed assuming full use of the available 7185 kg in LEO.

Previously it was mentioned that the red highlighted orbit in Fig. 3 (i.e. the natural orbit in Table 1) was selected as it appeared to be most favourable for designing optimal transfer trajectories. This becomes clear from Fig. 8 which shows the maximum mass that can be injected into any of the 80 manifolds of each of the orbits of the family of L_2 natural eight-shaped orbits. The figure also includes the minimum distance that is reached by any of the manifolds to clearly indicate the relation between the minimum approach distance and the mass that can be injected.[8]

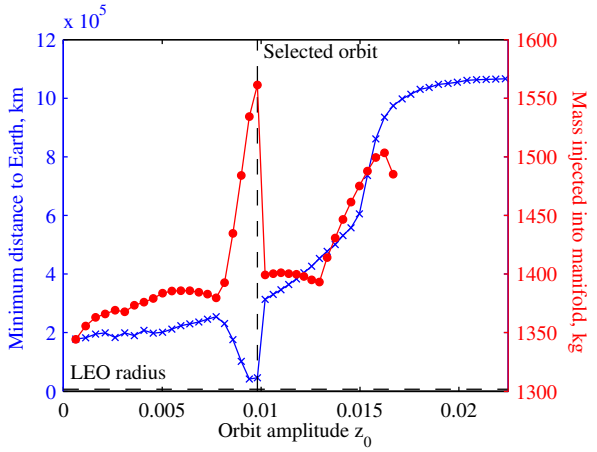

Fig. 8 Minimum Earth distance reached and maximum mass injected into any manifold of the natural L_2 family of eight-shaped orbits.

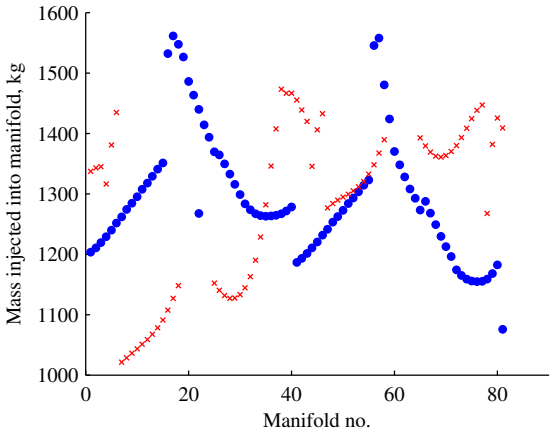

Fig. 9 Mass injected into the manifolds of the selected natural (blue round markers) and solar sail displaced (red cross markers) eight-shaped orbits.

Furthermore, for large enough z-amplitudes no solutions can be found as each of the manifolds of the eight-shaped orbits approach the Earth with an eccentricity larger than unity.

The best performing orbit in Fig. 8 has a z-amplitude of 0.0098 (the red highlighted orbit in Fig. 3) and allows for 1561 kg to be injected into the manifold. It must be noted however, that the target orbit of the near-Earth phase corresponding to this trajectory has a semi-major axis of 1.5 million km. The two-body approximation in the near-Earth phase is therefore not accurate. However, it can serve as a good initial guess.

To show the performance of the individual manifolds of the selected orbit, Fig. 9 is included (blue round markers), where the manifold number runs from the northern apex of the eight-shaped orbit, $t_o = 0$ and along the orbit until $t_o = P_o$ (with t_o the time in the eight-shaped orbit measured from the northern apex). The figure shows a rather large dependency of the performance on the particular manifold selected and the best performance for manifold number 17.

V.II SEP trajectories

Using the ballistic trajectories of the previous section as initial guess, the results for the use of SEP in the low-thrust arc can be generated. Those results are presented in Fig. 10 and detailed results can be found in Table 3. The results show that the use of SEP allows for a mass of 1564 kg to be injected into the natural eight-shaped orbit. This is only 3 kg more than the ballistic option. However, the SEP solution satisfies the boundary conditions defined in Eq. (16), which ensure the validity of the near-Earth model, while the ballistic solution does not.

Table 3 furthermore shows that the total transfer time from LEO is 478 days, which is substantial. An improvement of this time of flight could possibly be obtained by including the time of flight in the objective function using a weighted sum approach. However, this will clearly result in a decrease of the mass delivered to the eight-shaped orbit.

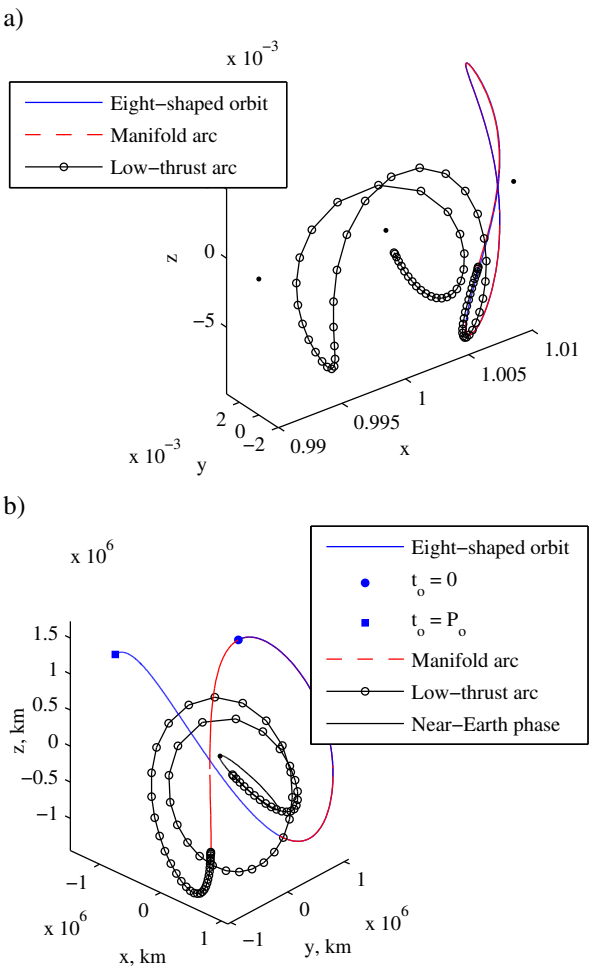

Fig. 10 Optimal SEP trajectory to natural eight-shaped orbit in a) the CR3BP reference frame and b) the Earth inertial reference frame.

Near-Earth phase	
Semi-major axis target orbit, km	488,641
Eccentricity target orbit	0.986
Inclination target orbit, deg	51.7
Time spent in near-Earth phase, days	39
Mass injected into interplanetary phase, kg	1583
Interplanetary phase	
Time spent in low-thrust arc, days	256
Mass injected into manifold, kg	**1564**
Manifold number	46
Time spent in manifold arc, days	183
Time in eight-shaped orbit at injection, t_o	0.624π

Table 3 Details of optimal SEP trajectory to natural eight-shaped orbit.

V.III Solar sail trajectories

Again, using the ballistic trajectories of Section V.I as initial guess, pure solar sail trajectories can be generated. Since for the solar sail trajectory the mass is constant throughout the low-thrust arc, the objective defined in Eq. (11) can be changed into $J = -f_{penalty} m_0$ with m_0 the mass at the start of the low-thrust arc or equivalently at the end of the near-Earth phase. The objective thus becomes to minimise the Fregat upper-stage propellant consumption in the near-Earth phase that is required to transfer the spacecraft from LEO to the target orbit. For that, the target orbit should be as similar as possible to LEO. This especially means driving the semi-major axis down and making sure that the inclination of the elliptic target orbit is equal to the LEO inclination (which the pure SEP trajectory already established, see Table 3).

To generate the results for the pure solar sail case, a range of sail lightness numbers are considered from $\beta_0 = 0.01$ to $\beta_0 = 0.05$. A continuation method is adopted to use the results from the previous value for β_0 as initial guess for the next value of β_0. The results are shown in Fig. 11 for $\beta_0 = 0.03$ and in Table 4 for other values of the sail lightness number.

Comparing the solar sail trajectory in Fig. 11 with the pure SEP trajectory in Fig. 10 shows a clear difference. In order to satisfy the constraint on the direction of the sail normal (see the third equation in Eq. (15)) and to maximise the use of the solar sail, the trajectory is directed away from the Sun, rather than towards the Sun as is the case for the pure SEP transfer. Furthermore, for increasing values of the lightness number, the mass injected into the eight-shaped orbit increases as can be expected, see Table 4. The reason for that is that a larger sail lightness number can establish a smaller semi-major axis and eccentricity of the target orbit and thus a larger mass injected into the interplanetary phase.

When computing the maximum thrust magnitude that the sail generates throughout the trajectory, it becomes clear that a lightness number of 0.02 is almost equivalent to the previously assumed SEP thrust magnitude of 0.2 N (for the considered spacecraft mass). A similar performance between the two types of propulsion should therefore be expected. However, this is not the case: 1589 kg for the solar sail case and 1564 kg for the SEP case. This can be explained by the propellant consumption by the SEP thruster since the mass at the start of the interplanetary phase is comparable for both cases: 1589 kg (solar sail) and 1583 kg (SEP). Still, a much better performance for the SEP case was expected as it is not limited in thrust direction like the solar sail. But apparently, this constraint does not have a limiting effect on the performance of the solar sail in this particular case. Then, the only advantage of SEP over solar sailing is the shorter time of flight: 478 days for the SEP case versus 570 days for the solar sail case, which is a decrease of 19 percent.

Finally, an estimation of the size of the solar sail required to deliver the optimised masses to the eight-shaped orbit is added to Table 4. Clearly, by increasing β_0 (and therefore also increasing the injected mass) the size of the solar sail increases. For the smallest value for β_0 of 0.01 a square sail with a side-length of 101 m is required, which increases to more than twice that size for a lightness number of 0.05.

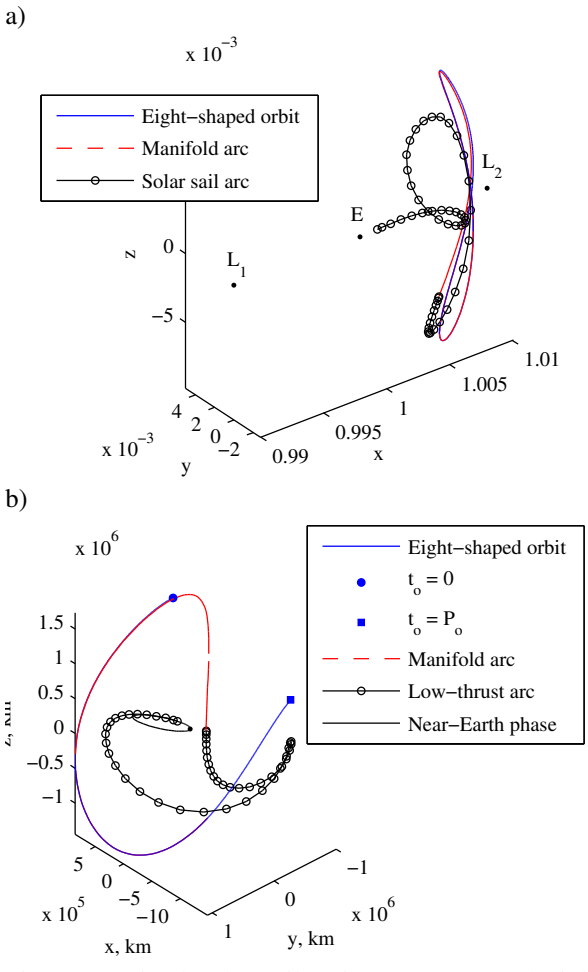

Fig. 11 Optimal solar sail trajectory to natural eight-shaped orbit for $\beta_0 = 0.03$ in a) the CR3BP reference frame and b) the Earth inertial reference frame.

β_0	Injected mass, kg	Equivalent thrust magnitude, N	Time of flight, days	Sail side-length, m
0.01	1574	0.068	592	101
0.02	1589	0.188	570	144
0.03	1593	0.280	492	176
0.04	1598	0.378	407	204
0.05	1602	0.473	432	229

Table 4 Details of optimal solar sail trajectory to natural eight-shaped orbit.

V.IV Hybrid propulsion trajectories

Using the pure solar sail trajectories as initial guess, but adding an SEP thruster to the optimal control problem, the results for the use of hybrid propulsion can be obtained. The main outcomes are provided in Table 5. Comparing the results with those for pure solar sailing in Table 4 shows only a very small increase in the performance for the hybrid case. This also becomes clear from comparing the actual optimal hybrid trajectory for a lightness number of 0.03 in Fig. 12 with the solar sail case in Fig. 11.

The slightly better performance of hybrid propulsion can be attributed to the contribution of the SEP thruster, for which the thrust profiles are provided in Fig. 13. These thrust profiles indicate that the SEP thruster is used only very limited. Apparently, using the SEP thruster cannot establish a significant gain in injected mass that outweighs the SEP propellant consumption.

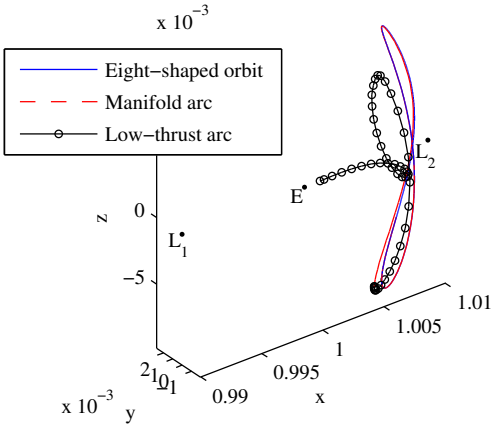

Fig. 12 Optimal hybrid trajectory to natural eight-shaped orbit for β_0 = 0.03 in the CR3BP reference frame.

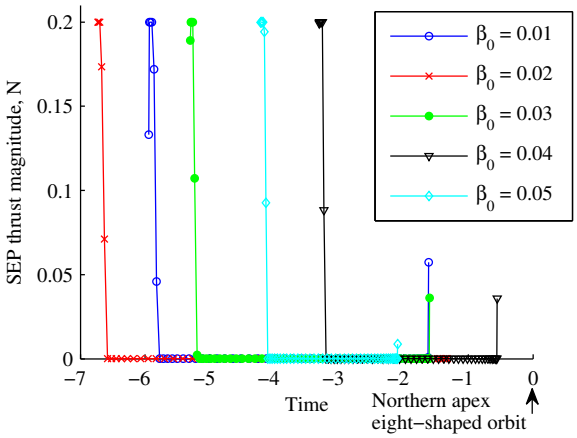

Fig. 13 SEP thrust profiles for optimal hybrid trajectories to natural eight-shaped.

β_0	0.01	0.02	0.03	0.04	0.05
Injected mass, kg	1579	1590	1595	1599	1603
Time of flight, days	516	547	465	400	365
Sail side-length, m	102	144	177	204	229

Table 5 Details of optimal hybrid trajectories to natural eight-shaped orbit.

Although the improved performance in terms of mass delivered to the eight-shaped orbit is not significant, the hybrid trajectories do allow for a shorter transfer time with respect to the pure solar sail case. On average, the transfer time is 40 days shorter, which is a decrease of 8 percent.

V.V Solar sail displaced eight-shaped orbits

A similar approach as used for the design of optimal low-thrust transfers to the selected natural eight-shaped orbit can be used to design optimal transfers to the selected sail displaced eight-shaped orbit (indicated by the blue round marker in Fig. 4). The ballistic results, where the near-Earth phase is patched to the point of closest approach of each of the 80 manifolds, are presented in Fig. 9 by the red cross markers. The maximum mass that can be injected into the eight-shaped orbit is 1473 kg by making use of manifold number 38.

Since a solar sail (with lightness number equal to 0.026) is available to generate the displaced eight-shaped orbit, the transfer is investigated for the same value for the lightness number. The results are provided

in Fig. 14 and Table 6. Comparing the injected mass with the mass injected into the natural eight-shaped orbit for a similar value of the lightness number shows that the transfer to the displaced eight-shaped orbit performs slightly less.

For comparison purposes, the transfer is also optimised for the use of SEP propulsion and hybrid propulsion. The results are shown in Table 7, which show a similar outcome as for the transfers to the natural eight-shaped orbit: the injected mass for the pure SEP case is smaller than for the pure solar sail case, while the hybrid case shows a very small improvement. Considering the time of flight, the pure SEP option performs best.

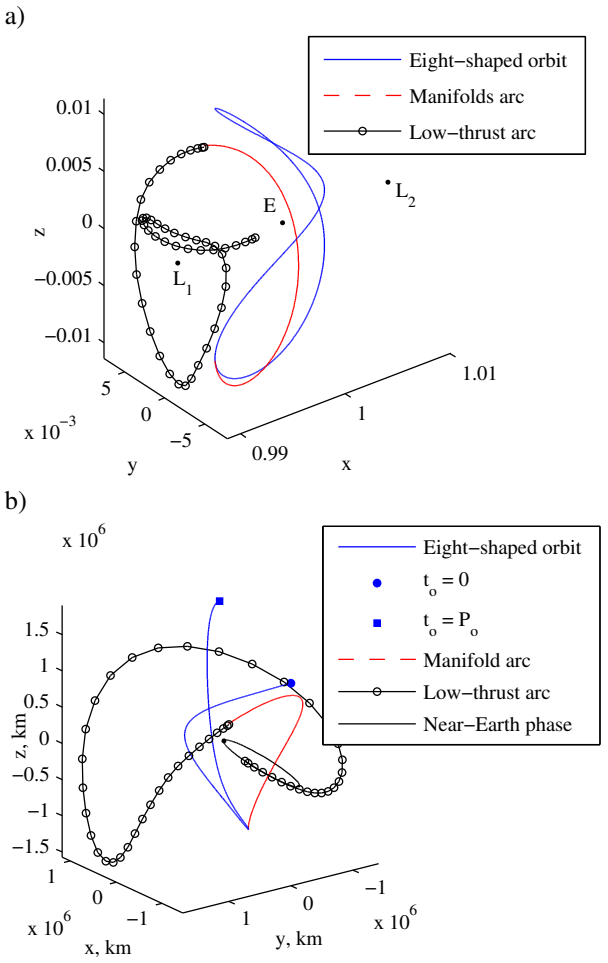

Fig. 14 Optimal solar sail trajectory to sail displaced eight-shaped orbit in a) the CR3BP reference frame and b) the Earth inertial reference frame.

β_0	Injected mass, kg	Equivalent thrust magnitude, N	Sail side-length, m	Time of flight, days
0.026	1576	0.171	164	510

Table 6 Details of optimal solar sail trajectory to sail displaced eight-shaped orbit.

Type of propulsion	SEP	Solar sail	Hybrid
Injected mass, kg	1538	1576	1578
Time of flight, days	383	510	475

Table 7 Optimised mass injected into the sail displaced eight-shaped orbit and time of flight for different propulsion options.

VI LOW-THRUST LAUNCH DESIGN APPROACH

The next step in the design of optimal low-thrust transfers to (displaced) eight-shaped orbits is replacing the high-thrust near-Earth phase with a low-thrust spiral. For this it is assumed that the optimal interplanetary phase obtained with the high-thrust near-Earth phase does not change. The objective thus becomes to find the optimal low-thrust steering law in each revolution of the spiral such that the spiral starts from LEO and ends at the target orbit defined by the initial state vector of the interplanetary phase. Since it can be expected that it will take many months to complete this spiral, the objective is to minimise the time of flight. To this end, locally optimal steering laws for the SEP thruster and solar sail are derived. Furthermore, an orbital averaging technique is employed to significantly reduce the computational cost for the integration of the equations of motion in the spiral.

VI.I SEP locally optimal steering law

The locally optimal control profile in the spiral for the SEP thruster is illustrated in Fig. 15 and assumes the following three steering laws in each revolution of the spiral:[26]

- To change the semi-major axis, a tangential steering law is applied around perigee over an angle $2p_s\pi$ using an in-plane acceleration, f_{in}.
- To change the eccentricity, an inertial steering law is applied where the spacecraft thrusts perpendicular to the line of apsides around apogee over an angle $2p_e\pi$ using an in-plane acceleration, f_{in}.
- To change the inclination, an out-of-plane steering law is applied around the nodal crossings over an

angle $p_i\pi$ with opposite thrusting direction along the ascending and descending nodes. An out-of-plane acceleration, f_{out}, is used to enable this law.

The controls in each revolution of the spiral are thus the in- and out-of-plane thrust accelerations, f_{in} and f_{out}, and the size of the tangential, inertial and out-of-plane thrusting arcs, p_s, p_e and p_i. Starting from Gauss' variational equations,[16] the effect of a particular steering law on the Keplerian elements after one orbital revolution can be computed by expressing the applied accelerations in radial, transversal and out-of-plane directions and integrating the resulting differential equations over the orbit period. Subsequently dividing by the orbit period (or 2π) provides the averaged equations of motion in the spiral. For conciseness, the full derivation is omitted, but can be found in the literature.[23, 26] Only the result is presented in Eq. (18).

$$
\begin{aligned}
\frac{da}{dE} &= \frac{1}{2\pi}\left(\frac{2a^3}{\mu_E} f_{in}\,\mathrm{sign}(p_s)\left[\sqrt{1-e^2}\,E+\left(1-\sqrt{1-e^2}\right)(0.5E-0.25\sin 2E)\right]_{E_{s,0}}^{E_{s,f}} + \frac{2a^3}{\mu_E} f_{in}\,\mathrm{sign}(p_e)\sqrt{1-e^2}\left[\sin E\right]_{E_{e,0}}^{E_{e,f}}\right)\\
\frac{de}{dE} &= \frac{1}{2\pi}\left(\frac{2a^2}{e\mu_E}\left(1-e^2\right) f_{in}\,\mathrm{sign}(p_s)\left(\frac{-e^2}{\sqrt{1-0.8e^2}}\left[0.5E+0.25\sin 2E\right]_{E_{s,0}}^{E_{s,f}} + \left[\ln\left(\sin E+\frac{1}{e}\sqrt{1-e^2\cos^2 E}\right)\right]_{E_{s,0}}^{E_{s,f}}\right.\right.\\
&\quad \left.\left. + \frac{a^2}{\mu_E} f_{in}\,\mathrm{sign}(p_e)\sqrt{1-e^2}\left[1.5E-2e\sin E+0.25\sin 2E\right]_{E_{e,0}}^{E_{e,f}}\right)\right.\\
\frac{di}{dE} &= \frac{1}{2\pi}\frac{a^2}{\mu_E} f_{out}\,\mathrm{sign}(p_i)\sum_{i=1}^{2}\left[\frac{\left(1+e^2\right)\cos\omega\sin E-1.5eE\cos\omega-0.25e\cos\omega\sin 2E}{\sqrt{1-e^2}}+\sin\omega\cos E-0.25e\sin\omega\cos 2E\right]_{E_{n_i,0}}^{E_{n_i,f}}\\
\frac{d\Omega}{dE} &= \frac{1}{2\pi}\frac{a^2}{\mu_E\sin i} f_{out}\,\mathrm{sign}(p_i)\sum_{i=1}^{2}\left[\frac{\left(1+e^2\right)\sin\omega\sin E-1.5eE\sin\omega-0.25e\sin\omega\sin 2E}{\sqrt{1-e^2}}-\cos\omega\cos E+0.25e\cos\omega\cos 2E\right]_{E_{n_i,0}}^{E_{n_i,f}}\\
\frac{d\omega}{dE} &= \frac{1}{2\pi}\left(\frac{-2a^2}{e^2\mu_E}\sqrt{1-e^2} f_{in}\,\mathrm{sign}(p_s)\left[\sqrt{1-e^2\cos^2 E}+\sin^{-1}(e\cos E)\right]_{E_{s,0}}^{E_{s,f}} + \frac{-a^2}{e\mu_E} f_{in}\,\mathrm{sign}(p_e)\left[0.25\cos 2E-e\cos E\right]_{E_{e,0}}^{E_{e,f}}\right)-\cos i\frac{d\Omega}{dE}\\
\frac{dm}{dE} &= -\frac{1}{2\pi}\frac{mf_{in}}{I_{sp}g_0}\frac{1}{n}\left(E_{s,f}-e\sin E_{s,f}-\left(E_{s,0}-e\sin E_{s,0}\right)+E_{e,f}-e\sin E_{e,f}-\left(E_{e,0}-e\sin E_{e,0}\right)\right)\\
&\quad -\frac{1}{2\pi}\frac{mf_{out}}{I_{sp}g_0}\frac{1}{n}\sum_{i=1}^{2}\left(E_{n_i,f}-e\sin E_{n_i,f}-\left(E_{n_i,0}-e\sin E_{n_i,0}\right)\right)
\end{aligned}
\tag{18}
$$

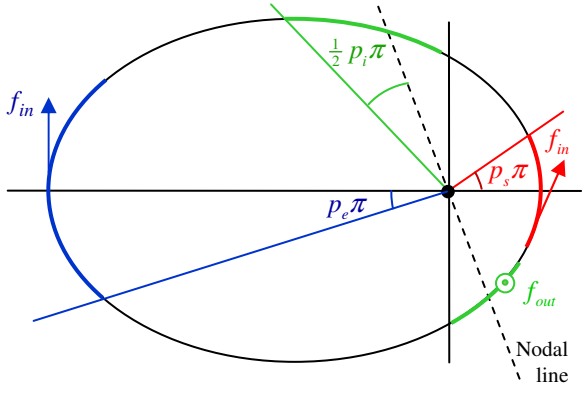

Fig. 15 Schematic of locally optimal SEP steering laws in near-Earth phase spiral.

Equation (18) makes use of the conventional Keplerian elements a, e, i, Ω, ω and the eccentric anomaly E, all defined in the Earth inertial reference frame of Fig. 6. μ_E is the gravitational parameter of the Earth and the subscripts '0' and 'f' indicate the initial and final value of the eccentric anomalies E_s, E_e and $E_{n,i}$ during which the tangential, inertial and out-of-plane steering laws occur, respectively. Finally, the sign of the control parameters p_s, p_e and p_i indicate whether the respective orbital element is increased or decreased.

VI.II Solar sail locally optimal steering law

Due to the constraint that the sail cannot generate an acceleration component in the direction of the Sun, the steering law adopted for the SEP thruster cannot be applied for the solar sail. Instead, a locally optimal energy-gain control strategy is applied.[17, 27, 28] The idea is to maximise the projection of the solar sail normal vector onto the instantaneous velocity vector, thereby maximising the energy rate of change along the trajectory. The control law that describes this is given by:[17, 28]

$$\tan\alpha = \frac{-3 \pm \sqrt{9 + 8\tan^2\tilde{\alpha}}}{4\tan\tilde{\alpha}} \tag{19}$$

with α the optimum cone angle of the solar sail normal vector, **n**, and $\tilde{\alpha}$ the cone angle of the velocity vector, **v**. The cone angle is defined as the angle between **n** or **v** and the instantaneous Sun-sail line, $\hat{\mathbf{r}}_s$, see Fig. 16. The latter is defined in the reference frame of Fig. 6 as:

$$\hat{\mathbf{r}}_s = \begin{pmatrix} \cos i_{obl} \cos t \\ \sin t \\ \sin i_{obl} \cos t \end{pmatrix} \tag{20}$$

with i_{obl} the obliquity of the ecliptic and t the dimensionless time during the year measured from the winter solstice. Besides satisfying Eq. (19), the sail normal should be contained in the plane spanning $\hat{\mathbf{r}}_s$ and **v**. Finally, the ± sign should be employed in such a way that the sail normal vector always points in the direction of the velocity vector, rather than opposite to it in order to ensure a maximum change in the orbital energy.

Since the cone angle of the velocity vector varies along the orbit, so does the optimal sail cone angle and the solar sail acceleration. The acceleration in the reference frame of Fig. 6 is given by:

$$\mathbf{a}_s = \beta_0 \frac{m_0}{m} \frac{\mu_S}{r_s^2} \cos^2\alpha \mathbf{n} \tag{21}$$

with μ_S the gravitational parameter of the Sun and r_s the Sun-sail distance, which is approximated by a constant value of 1 Astronomical Unit. By subsequently converting the acceleration in Eq. (21) from the Cartesian reference frame in Fig. 6 to a reference frame in radial, transversal and out-of-plane directions, the acceleration can be substituted into Gauss' variational equations. The instantaneous rate of change of the orbital elements due to the solar sail acceleration is then known. By finally discretising the orbit in a number of nodes, computing the instantaneous rate of change of the orbital elements at each node and using trapezoidal integration, the change in orbital elements after one orbital revolution can be obtained. The averaged equations of motion due to the solar sail are thus given through:

$$\frac{d\mathbf{x}_{oe}}{dE} = \frac{1}{2\pi}\left(\frac{\Delta E}{2}\sum_{k=1}^{N}\left(\left.\frac{d\mathbf{x}_{oe}}{dE}\right|_{k+1}\left(\mathbf{x}_{oe},\hat{\mathbf{r}}_s\right) + \left.\frac{d\mathbf{x}_{oe}}{dE}\right|_{k}\left(\mathbf{x}_{oe},\hat{\mathbf{r}}_s\right)\right)\right) \tag{22}$$

with $\mathbf{x}_{oe}$ the state vector of orbital elements in the Earth inertial reference frame of Fig. 6, N the number of discretisation nodes and $\Delta E = 2\pi(N\text{-}1)$. Equation (22) furthermore shows that the instantaneous rate of change of the orbital elements is only a function of the current state vector and the direction of the Sun-sail line. Note that the orbital elements are assumed constant throughout one revolution as is done for the locally optimal SEP steering law in the previous section.

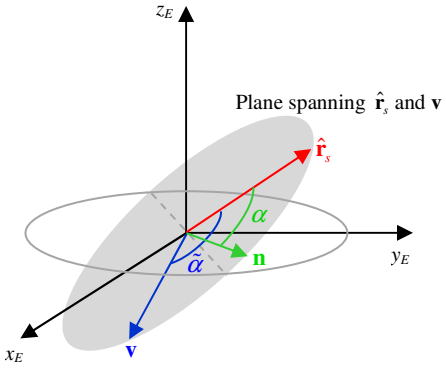

Fig. 16 Definition of velocity cone angle and optimal solar sail cone angle in reference frame of Fig. 6.

VI.III Optimal control problem - SEP

Although the optimal control problem to be solved in the low-thrust spiral is quite similar for both the use of pure SEP and for hybrid propulsion, some essential differences exist. Therefore, first the optimal control problem for the pure SEP case will be provided and subsequently the required adaptations for the hybrid case will be discussed.

As stated before, the objective is to minimise the time of flight in the spiral:

$$J = t_f - t_0 \tag{23}$$

where the time is the seventh state in the state vector:

$$\mathbf{x} = \left[\mathbf{x}_{oe} \quad m \quad t\right]^T = \left[a \quad e \quad i \quad \Omega \quad \omega \quad m \quad t\right]^T \tag{24}$$

The time variable is thus not the independent variable. Instead, the eccentric anomaly is taken as independent variable. This is done because PSOPT uses a Lagrange-Gauss-Lobatto distribution to discretise the interval of the independent variable, which results in a larger concentration of nodes at the start and end of that interval. With the orbital period in the last few revolutions expected to be very long, choosing time as the independent variable could give rise to multiple nodes per revolution. Theoretically this means that the control profile can change over these last few nodes, leading to different steering laws, and consequently

different equations of motion, within the same revolution. When using the eccentric anomaly as time variable, this problem does not occur since each revolution of the spiral takes an equal portion of the independent variable interval and with hundreds of spiral revolutions, the chance of multiple nodes in the last few spiral revolutions becomes negligible.

The control vector consists of the controls determining the SEP steering laws:

$$\mathbf{u} = \begin{bmatrix} p_s & p_e & p_i & T_{in} & T_{out} \end{bmatrix}^T \tag{25}$$

with bounds as follows:

$$\begin{aligned} \mathbf{-1} \leq \begin{bmatrix} p_s & p_e & p_i \end{bmatrix}^T \leq \mathbf{1} \\ \mathbf{0} \leq \begin{bmatrix} T_{in} & T_{out} \end{bmatrix}^T \leq \mathbf{T_{max}} \end{aligned} \tag{26}$$

with $T_{\max} = 0.2$ N.

The equations of motion are given by Eq. (18) and an additional equation that accounts for the change in the time variable. Since the assumption is made that the orbital elements do no change within one orbital revolution, the differential equation for the time can be computed as the averaged orbital period:

$$\frac{dt}{dE} = \frac{P}{2\pi} = \sqrt{\frac{a^3}{\mu_E}} \tag{27}$$

The event constraints can be defined as:

$$\begin{aligned} \mathbf{x}_0 &= \begin{bmatrix} a_{LEO} & e_{LEO} & i_{LEO} & \Omega_0 & \omega_0 & m_0 & t_0 \end{bmatrix}^T \\ \mathbf{x}_f &= \begin{bmatrix} a_{i,0} & e_{i,0} & i_{i,0} & \Omega_{i,0} & \omega_{i,0} & m_{i,0} & t_{i,0} \end{bmatrix}^T \end{aligned} \tag{28}$$

with the initial right ascension of the ascending node, argument of perigee, time and mass free. The subscript 'LEO' indicates the conditions in the 200 km altitude LEO (see Table 2) and the subscript '*i*,0' indicates the conditions at the start of the optimised interplanetary transfer. Note that the mass at the start of the spiral is free, but that the mass at the end of the spiral should equal the mass at the start of the interplanetary transfer phase as determined in Section V.

Finally, two path constraints need to be taken into account:

$$\begin{aligned} |p_s| + |p_e| \leq 1 \\ \sqrt{T_{in}^2 + T_{out}^2} \leq T_{\max} \end{aligned} \tag{29}$$

where the first path constraint ensures that the thrust arcs for tangential and inertial steering do not overlap.

Initial guesses for the pure SEP spiral can be found by assuming constant values for the elements of the control vector, integrating the averaged equations of motion and updating the control values through an iterative approach to satisfy the event constraints on the final state vector.

VI.IV Optimal control problem – hybrid propulsion

In order to incorporate the solar sail in the optimal control problem, the following two changes have to be made. First, the dynamics of the solar sail (see Eq. (22)) need to be added to the dynamics of the SEP thruster in Eq. (18). Second, the constraint on the inclination at the start of the hybrid spiral has to be removed, which means that the inclination can be different from the 51.8° as used for the LEO so far. The reason for this is the fact that the solar sail cannot generate an acceleration that is purely in the plane of the LEO and the start of the interplanetary phase (which is very close to 51.8°, see for example Table 3). This means that an out-of-plane component exists which has to be cancelled by the SEP thruster if the constraint on the initial inclination is included. The result is a longer spiral time (as less SEP thrust can be used for increasing the orbital energy) and a higher propellant consumption. If instead the initial inclination is free, the out-of-plane component of the solar sail does not need to be counterbalanced by the SEP thruster but can be used to eventually wind onto the 51.8° plane. The only disadvantage of this approach is that the Fregat upper-stage will have to change the LEO inclination of 51.8° to the new inclination at the start of the hybrid spiral. This can be quite costly. However, the Soyuz launch vehicle can also launch the spacecraft into three different LEO inclinations, namely 64.9°, 70.4° and 95.4° with performances of 6449 kg, 6294 kg and 6275 kg, respectively.[24] As will become clear later on, launching into one of these alternative parking orbits can be advantageous.

Besides these two changes, the optimal control problem as defined for the use of SEP remains unchanged, including the definition of the controls. This means that no controls need to be added in the case of hybrid propulsion as the steering law of the solar sail is given by the current state vector only. The contribution of the solar sail to the optimal control problem can thus be seen as a constant perturbing term in the equations of motion.

Finally it is noted that for the hybrid case, the optimal SEP spiral serve as initial guess.

VI.V Results

This section presents the results of both SEP and hybrid spirals for the SEP and hybrid interplanetary phases. Only the transfers to the natural eight-shaped orbit is considered as similar results can be expected for the transfers to the sail displaced eight-shaped orbits.

SEP spirals

The results for using a pure SEP spiral to connect the LEO with either the SEP or hybrid interplanetary phase are provided in Table 8 and in Fig. 17 for a pure SEP interplanetary phase. The table shows that through the use of an SEP spiral the mass required in LEO is only approximately 3100 kg compared to 7185 kg for the case of a Fregat upper-stage near-Earth phase. Clearly, this reduction comes at the cost of an increase in the time of flight. While the near-Earth phase takes tens of days for the Fregat upper-stage to complete, it takes over 800 days for the SEP spiral. A method to significantly reduce this transfer time would be by clustering multiple SEP thrusters. For example, by using two thrusters, increasing the maximum thrust magnitude to 0.4 N, the spiral time can be halved without a penalty on the mass required in LEO.

β_0 in inter-planetary phase	Mass required in LEO (incl. Fregat + adapter), kg	Mass end spiral/start interplanetary phase, kg	Time of flight in spiral, days
0 (SEP)	3104	1583	1060
0.01	3109	1582	1012
0.02	3129	1593	918
0.03	3131	1597	893
0.04	3137	1602	882
0.05	3140	1606	862

Table 8 Details of optimal SEP near-Earth spiral phase for the SEP and hybrid interplanetary phases.

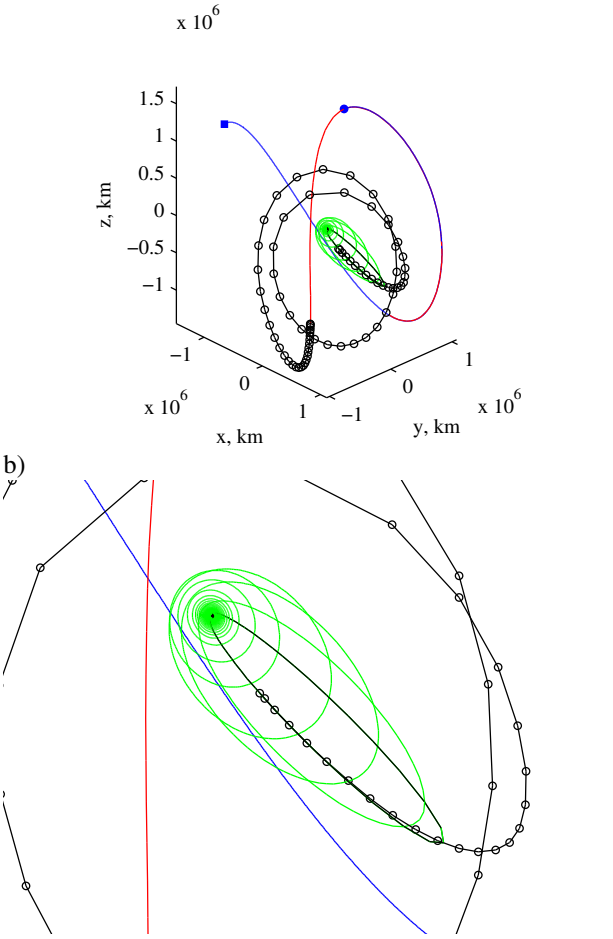

Fig. 17 Optimal SEP transfer to natural eight-shaped orbit in Earth inertial reference frame including the low-thrust SEP spiral from LEO. a) Full transfer. b) Close-up of spiral. Note that not all revolutions of the spiral are depicted for clarity.

Hybrid spirals

To show the advantage of using hybrid propulsion in the spiral over the use of pure SEP, this subsection shows the result of a hybrid spiral for the case of β_0 = 0.03. An overview of the results is provided in Table 1, Fig. 18 and Fig. 19, which include the results for the pure SEP spiral of Table 8 for comparison.

The table shows that, by removing the constraint on the inclination at the start of the spiral, an initial spiral inclination of 72.5° results. This larger inclination also becomes clear from the evolution of the orbital elements in Fig. 18a and from Fig. 19b-c which show the spiral when viewed parallel to the 51.8° plane. The latter figure shows that the SEP spiral is fully contained in the 51.8° plane while the hybrid spiral starts from a much

larger inclination and slowly winds onto the 51.8° plane. The consequence is that the Fregat upper-stage has to change the LEO inclination from 51.8° to 72.5°. For a spacecraft mass of 1928 kg (see Table 9), this requires the maximum available mass of 7185 kg in the 51.8° LEO. This is significantly larger than the 3129 kg required for the SEP spiral and does not provide an improvement over the use of the Fregat upper-stage. However, as indicated previously, the Fregat upper-stage can also launch the spacecraft into a 70.4° LEO. In that case, the mass required in LEO is only 3306 kg. Compared to the SEP spiral this is an increase of only 175 kg, but enables a saving in the spiral time of 174 days: 893 days for an SEP spiral and 744 days for a hybrid spiral. Additionally, the hybrid spiral allows for a saving in propellant consumption of 103 kg, which is also evident from the shorter thrust profiles in Fig. 18b.

	SEP spiral	Hybrid spiral
Inclination start spiral, deg	51.8	72.5
Mass required in 51.8° LEO, kg	3129	7185
Mass required in 70.4° LEO, kg	n.a.	3306
Time of flight in spiral, days	893	744
Mass start spiral, kg	2031	1928
Propellant consumption in spiral, kg	434	330

Table 9 Details of optimal hybrid (β_0 = 0.03) near-Earth spiral phase compared to a pure SEP spiral.

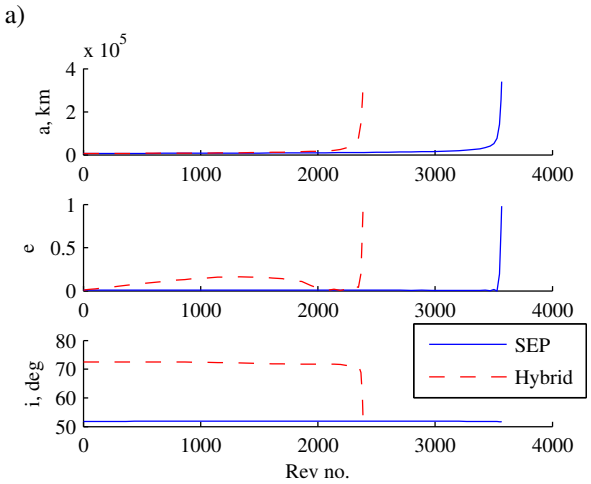

b)

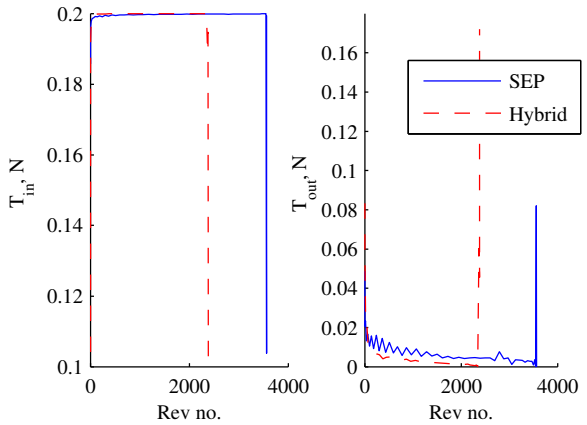

Fig. 18 Evolution of orbital elements (a) and in- and out-of-plane SEP thrust magnitudes (b) for optimal hybrid spiral (β_0 = 0.03) towards the natural eight-shaped orbit.

a)

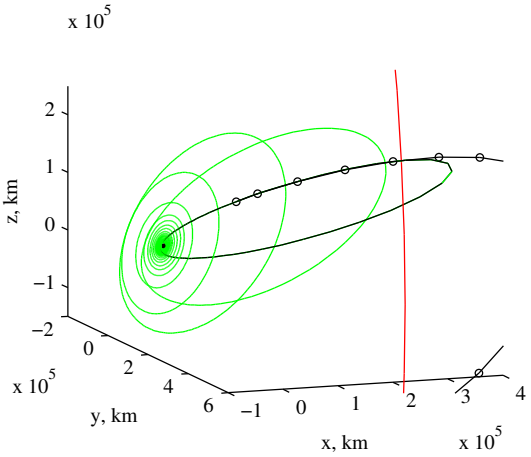

b) c)

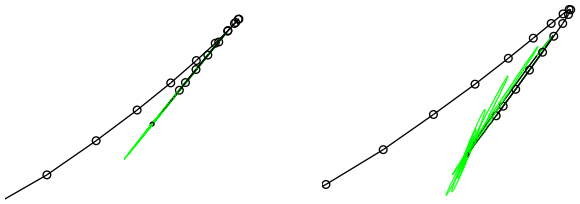

Fig. 19 a) Optimal hybrid spiral (β_0 = 0.03) towards the natural eight-shaped orbit in the Earth inertial reference frame. b-c) Close-up view parallel to LEO of SEP (b) and hybrid (c) spiral.

VII CONCLUSIONS

In this paper, optimal low-thrust transfers to eight-shaped orbits in the circular restricted three body problem have been investigated. These orbits are of special interest for high-latitude Earth observation and telecommunications. Different propulsion technologies, including solar electric propulsion (SEP), solar sailing and hybridised SEP and solar sailing have been investigated. Using both a high-thrust Fregat upper-stage launch phase and a low-thrust spiral launch, the mass injected into the eight-shaped orbit has been optimised. For this, the manifolds that wind onto the eight-shaped orbits are exploited. Finally, transfers to both natural and a solar sail displaced eight-shaped orbits have been considered.

Regarding the case of using the Fregat upper-stage, the mass injected into the natural eight-shaped orbit is at least 1564 kg. The pure SEP case (1564 kg) provides the smallest mass delivered, but allows for the shortest transfer times (478 days). Hybrid propulsion can establish a slightly better performance (1579-1603 kg, depending on the sail lightness number). The performance of hybrid propulsion is very similar to the performance of the pure solar sail transfers, but require shorter transfer times: 365-547 days for hybrid transfers versus 407-592 days for solar sail transfers. Overall, slightly smaller masses can be injected into the sail displaced eight-shaped orbit (a maximum of 1578 kg for the hybrid case) but for similar time of flights. Regarding the low-thrust spiral launch, an SEP or hybrid spiral can significantly reduce the mass required in low-Earth orbit for injecting the same amount of mass into the eight-shaped orbit: while the use of the Fregat upper-stage requires 7185 kg in LEO, the use of an SEP spiral requires only 3104-3140 kg. Clearly, this comes at the cost of an increase in the time of flight: while the Fregat takes only tens of days to deliver the spacecraft to the interplanetary phase of the transfer, the SEP spiral requires at least 862 days. This can be reduced significantly by considering a hybrid low-thrust spiral. A reduction in the time of flight of 17 percent can be established for only a 3 percent increase in the mass required in LEO.

ACKNOWLEDGEMENTS

This work was funded by the European Research Council Advanced Investigator Grant - 227571: VISIONSPACE: Orbital Dynamics at Extremes of Spacecraft Length-Scale.

REFERENCES

[1]. Lazzara, M. A., Coletti, A., and Diedrich, B. L. "The possibilities of polar meteorology, environmental remote sensing, communications and space weather applications from Artificial Lagrange Orbit," *Advances in Space Research* Vol. 48, No. 11, 2011, pp. 1880-1889. Doi: 10.1016/j.asr.2011.04.026

[2]. Gautier, D. L., Bird, K. J., Charpentier, R. R., Grantz, A., Houseknecht, D. W., Klett, T. R., Moore, T. E., Pitman, J. K., Schenk, C. J., Schuenemeyer, J. H., Sørensen, K., Tennyson, M. E., Valin, Z. C., and C.J., W. "Assessment of Undiscovered Oil and Gas in the Arctic," *Science* Vol. 324, No. 5931, 2009, pp. 1175-1179. Doi: 10.1126/science.1169467

[3]. Johannessen, O. M., Alexandrov, V. Y., Frolov, I. Y., Sandven, S., Pettersson, L. H., VBobylev, L. P., Kloster, K., Smirnov, V. G., Mironov, Y. U., and Babich, N. G. *Remote Sensing of Sea Ice in the Northern Sea Route - Studies and Applications*. Chichester, UK: Praxis Publishing LtD, 2007.

[4]. Anderson, P., and Macdonald, M. "Extension of the Molniya Orbit Using Low-Thrust Propulsion," *21st AAS/AIAA Space Flight Mechanics Meeting, AAS 11-236*. New Orleans, USA, 2011.

[5]. Heiligers, J., Ceriotti, M., McInnes, C. R., and Biggs, J. D. "Mission Analysis and Systems Design of a Near-term and Far-term Pole-sitter Mission," *1st IAA Conference on Dynamics and Control of Space Systems*. Porto, Portugal, 2012.

[6]. Forward, R. L. "Statite: A spacecraft that does not orbit," *Journal of Spacecraft and Rockets* Vol. 28, No. 5, 1991, pp. 606-611. Doi: 10.2514/3.26287

[7]. Waters, T. J., and McInnes, C. R. "Periodic Orbits Above the Ecliptic in the Solar-Sail Restricted Three-Body Problem," *Journal of Guidance, Control, and Dynamics* Vol. 30, No. 3, 2007, pp. 687-693. Doi: 10.2514/1.26232

[8]. Ceriotti, M., and McInnes, C. "Natural and sail-displaced doubly-symmetric Lagrange point orbits for polar coverage," *Celestial Mechanics and Dynamical Astronomy*, 2012. Doi: 10.1007/s10569-012-9422-2

[9]. Kazantzis, P. G. "Numerical determination of families of three-dimensional double-symmetric periodic orbits in the restricted three-body problem. I.," *Astrophysics and Space Sciences* Vol. 65, 1979, pp. 493-513. Doi: 10.1007/BF00648513

[10]. Kazantzis, P. G. "Numerical determination of families of three-dimensional double-symmetric periodic orbits in the restricted three-body problem. II.," *Astrophysics and Space Sciences* Vol. 69, 1980, pp. 353-368. Doi: 10.1007/BF00661923

[11]. Senent, J., and Ocampo, C. "Low-Thrust Variable-Specific-Impulse Transfers and Guidnace to Unstable Periodic Orbits," *Journal of Guidance, Control, and Dynamics* Vol. 28, No. 2, 2005, pp. 280-290. Doi: 10.2514/1.6398

[12]. Mengali, G., and Quarta, A. A. "Trajectory Design with Hybrid Low-Thrust Propulsion System," *Journal of Guidance, Control, and Dynamics* Vol. 30, No. 2, 2007, pp. 419-426. Doi: 10.2514/1.22433

[13]. Baig, S., and McInnes, C. R. "Artificial Three-Body Equilibria for Hybrid Low-Thrust Propulsion," *Journal of Guidance, Control, and Dynamics* Vol. 31, No. 6, 2008, pp. 1644-1655. Doi: 10.2514/1.36125

[14]. Heiligers, J., Ceriotti, M., McInnes, C. R., and Biggs, J. D. "Displaced Geostationary Orbit Design Using Hybrid Sail Propulsion," *Journal of Guidance, Control, and Dynamics* Vol. 34, No. 6, 2011, pp. 1852-1866. Doi: 10.2514/1.53807

[15]. Ceriotti, M., and McInnes, C. R. "Generation of Optimal Trajectories for Earth Hybrid Pole Sitters," *Journal of Guidance, Control, and Dynamics* Vol. 34, No. 3, 2011, pp. 847-859. Doi: 10.2514/1.50935

[16]. Battin, R. H. *An Introduction to the Mathematics and Methods of Astrodynamics, Revised Edition*. Reston, USA: American Institute of Aeronautics and Astronautics, Inc., 1999.

[17]. McInnes, C. R. *Solar Sailing: Technology, Dynamics and Mission Applications*. Berlin: Springer-Praxis Books in Astronautical Engineering, Springer-Verlag, 1999.

[18]. EADS Astrium. "EADS Astrium Ion Propulsion Systems." Retrieved from http://cs.astrium.eads.net/sp/spacecraft-propulsion/ion-propulsion/index.html, 10 June 2012.

[19]. Dachwald, B., Mengali, G., Quarta, A. A., and Macdonald, M. "Parametric Model and Optimal Control of Solar Sails with Optical Degradation," *Journal of Guidance, Control, and Dynamics* Vol. 29, No. 5, 2006, pp. 1170-1178. Doi: 10.2514/1.20313

[20]. McInnes, C. R., McDonald, A. J., Simmons, J. F. L., and MacDonald, E. W. "Solar Sail Parking in Restricted Three-Body Systems," *Journal of Guidance, Control, and Dynamics* Vol. 17, No. 2, 1994, pp. 399-406. Doi: 10.2514/3.21211

[21]. Koon, W. S., Lo, M. W., Marsden, J. E., and Ross, S. D. *Dynamical Systems, the Three-Body Problem and Space Mission Design*, 2006.

[22]. Howell, K. C. "Families of orbits in the vicinity of the collinear libration points," *Journal of the Astronautical Sciences* Vol. 49, No. 1, 2001, pp. 107-125.

[23]. Heiligers, J., Ceriotti, M., McInnes, C. R., and Biggs, J. D. "Design of optimal Earth pole-sitter transfers using low-thrust propulsion " *Acta Astronautica* Vol. 79, 2012, pp. 253-268. Doi: 10.1016/j.actaastro.2012.04.025

[24]. Starsem "The Soyuz Company". "Soyuz User's Manual (ST-GTD-SUM-01 - issue 3 - revision 0)." 2001.

[25]. Becerra, V. M. "Solving complex optimal control problems at no cost with PSOPT," *IEEE Multi-conference on Systems and Control*,Yokohama, Japan, 2010, pp. 1391-1396.

[26]. Gao, Y. "Near-Optimal Very Low-Thrust Earth-Orbit Transfers and Guidance Schemes," *Journal of Guidance, Control, and Dynamics* Vol. 30, No. 2, 2007, pp. 529-539. Doi: 10.2514/1.24836

[27]. Macdonald, M., and McInnes, C. R. "Realistic Earth Escape Strategies for Solar Sailing," *Journal of Spacecraft and Rockets* Vol. 28, No. 2, 2004, pp. 315-323. Doi: 10.2514/1.5165

[28]. Coverstone, V. L., and Prussing, J. E. "Technique for Escape from Geosynchronous Transfer Orbit Using a Solar Sail," *Journal of Guidance, Control, and Dynamics* Vol. 26, No. 4, 2003, pp. 628-634. Doi: 10.2514/2.5091